Tribology Letters (2019) 67:21
https://doi.org/10.1007/s11249-019-1134-2

METHODS

AFM at the Macroscale: Methods to Fabricate and Calibrate Probes for Millinewton Force Measurements

N. T. Garabedian[1] · H. S. Khare[2,3] · R. W. Carpick[2] · D. L. Burris[1]

Received: 15 November 2018 / Accepted: 2 January 2019 / Published online: 7 January 2019

Abstract

The difficulty in detecting and controlling forces in the gap between the nanoscale and macroscale tribometry regimes has so far limited the application of fundamental atomic-scale insights to practical friction and wear control. This paper describes methods to achieve and quantify millinewton forces measured by atomic force microscopy (AFM) using existing experimental tools. We mounted colloidal microspheres at different points along the span of commercial AFM cantilevers to reduce their effective flexural length from 125 μm to between 21 and 107 μm. The resulting spring constants, based on direct calibration, varied from 100 to 10,000 N/m. Within a commercial AFM (Dimension 3100), these cantilevers produced normal force calibration constants between 0.006 and 0.430 mN/V; i.e., increasing the spring constant by 100 × caused a corresponding increase in the calibration constant but only a negligible increase in V/m sensitivity. We demonstrate these new capabilities by measuring friction between the colloids and single-crystal MoS_2 at applied normal forces up to 3.4 mN, which is in the range of existing tribometers and well above the forces typically used in AFM-based measurements. These methods, which make use of well-established procedures and only require a modified AFM cantilever, are intended for use by other researchers as a platform for bridging the gap between nanoscale and macroscale tribometry.

Keywords High-force AFM · Normal force calibration · AFM colloidal probes · AFM reference cantilevers

1 Introduction

Macroscale tribological contacts typically comprise many discrete nanoscale contact areas of unknown; location-dependent; and time-varying size, shape, and pressure [1]. In addition to effects from deformation, wear, third bodies, and tribofilm growth, these features make controlled studies of macroscale tribological phenomena especially difficult [2]. By contrast, nanoscale friction measurements, which typically use atomic force microscopy (AFM), can be conducted within a single asperity contact of well-defined size and location to promote more fundamental studies of tribological phenomena [3–5]. In one of the pioneering examples [6], the spatial periodicity of stick–slip friction variations matched the lattice structure of the graphite substrate as predicted by the Prandtl-Tomlinson model of atomic-scale friction [7, 8]. Other investigators have since used scanning probe microscopy (SPM) to study lattice periodicity [9–11], frictional anisotropy [12, 13], contaminant effects, superlubricity [12, 14, 15], and thermally activated slip [10, 16–21] among other fundamental aspects of atomic-scale friction. More recently, large-scale molecular dynamics (MD) simulation have been used to model these nanoscale tribological interactions and strengthen the link between experimentally observable phenomena [7, 22] and their underlying mechanisms [23].

It remains unclear how these fundamental nanotribological phenomena manifest themselves at the larger loads and length scales of more typical tribological contacts. Yoon et al. studied frictional scaling by comparing the frictional response of Si and DLC to varying probe radius using low loads in the AFM and high loads in a microtribometer [24]. Interestingly, AFM-based friction coefficients of both materials increased with probe radius toward the

✉ D. L. Burris
dlburris@udel.edu

[1] Department of Mechanical Engineering, University of Delaware, Newark, DE, USA

[2] Department of Mechanical Engineering & Applied Mechanics, University of Pennsylvania, Philadelphia, PA, USA

[3] Present Address: Department of Mechanical Engineering, Gonzaga University, Spokane, WA 99258, USA

radius-independent values obtained by the microtribometer. Nonetheless, the friction coefficients, probe radii, and loads differed by 10×, 100× and 10,000×, respectively, between instruments. Bhushan and Kulkarni varied load at constant probe radius and attributed a transition from lower friction coefficients at lower loads to higher friction coefficients at higher loads to the onset of plastic deformation and wear [25]. Tambe and Bhushan [26] and Bhushan et al. [27] conducted similar experiments for a range of materials using AFM and microtribometry and showed that microscale friction coefficients were typically an order of magnitude greater than their nanoscale counterparts. They proposed that increased plastic deformation, reduced hardness, third bodies (wear) and roughness contributed to the relatively larger friction coefficients of the microscale contacts. While these results demonstrate clear differences between nano- and microscale friction, they fail to elucidate where these differences first emerge; why they occur; if they are dominated by differences in contact size, load, contact stresses, or sliding speed [28]; and if the trend of increased friction with size scale is an inherent feature of all or most tribological systems.

Understanding how fundamental atomic-scale interactions ultimately contribute to macroscale friction and wear requires controlled studies of friction across the relevant length and load scales. Experimental limitations, primarily in load control and sensing, have precluded such studies to date. In this paper, we develop general methods to help close this experimental gap. Because all commercial AFM's infer forces based on beam deflection measurements, the range of loads that can be applied and measured is primarily limited by the stiffness of the cantilever. Herein, we describe: (1) how well-established probe mounting methods can be used to increase the load range of commercial AFMs beyond 1 mN, which is within the range of existing microtribometers; (2) a direct method to calibrate beam stiffness and quantify AFM forces in the millinewton testing regime; and (3) the validation of a high-force AFM measurement approach using a commercial instrument and a model tribological system.

2 Materials and Methods

2.1 Preparation of High-Force AFM Cantilevers

Silicon tapping mode cantilevers (with a nominal stiffness of 40 N/m) were used and customized in this study. According to the Euler beam theory, cantilever beam stiffness is inversely proportional to the cube of distance between the fixed end and the loading point; the "effective length" is hereafter defined as the distance between the fixed end and the center of the colloid as illustrated in Fig. 1. Using methods described in our recent paper [29], we mounted ~ 30 µm steel microspheres (NanoSteel Co., Providence RI) at controlled distances along the span of the cantilevers to systematically vary the effective length, spring constant, force constant, and load capacity of otherwise stock AFM cantilevers.

The colloidal spheres were mounted at varying locations along the cantilever using a two-part epoxy (JB Weld, Sulphur Springs TX) with the aid of an optical microscope and a custom micromanipulator, based on previously established methods [30]. Optical images of the seven mounted cantilevers prepared for this study are shown in Fig. 1. The measured dimensions and properties of these beams are provided in Table 1.

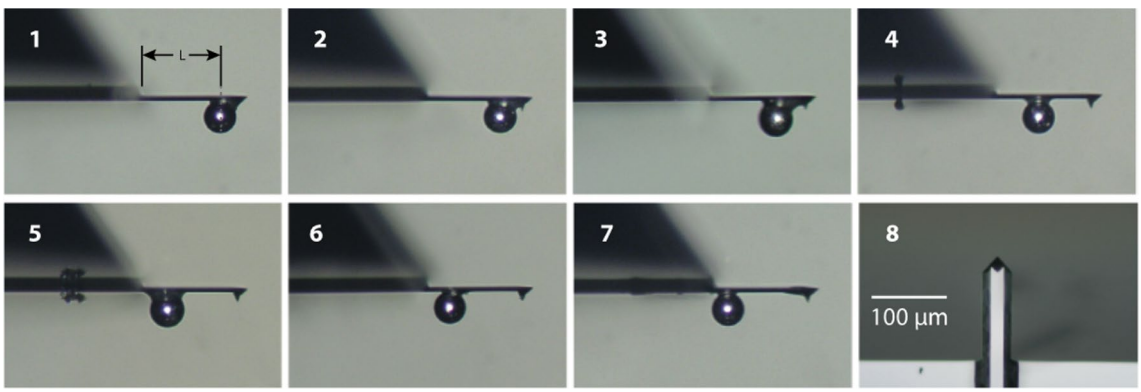

Fig. 1 (1–7) Profile views of the seven cantilevers prepared for this study. The distance of the steel colloid from the free end of 40 N/m cantilevers decreases with increased cantilever number. These optical images were subsequently used for determining the effective length, as illustrated in (1), following mounting of steel colloids; (8) an illustrative plan-view of an unmodified cantilever used to quantify the lateral dimensions (length and width) of the cantilever. All eight images have the same scale

Table 1 Measured properties of the seven cantilevers used in this study

	Cantilever						
	No. 1	No. 2	No. 3	No. 4	No. 5	No. 6	No. 7
Beam width (long base) (μm)	37.3	36.4	35.9	37.4	36.6	36.1	37.8
Beam width (short base) (μm)	17.2	17.2	17.0	17.4	17.7	17.3	17.8
Thickness (μm)	5.0	5.0	5.0	5.0	5.0	5.0	5.0
Effective beam length (μm)	106.9	98.1	88.5	55.9	31.3	30.2	21.1
Measured stiffness, $k_{\text{cantilever}}$ (N/m)	78 ± 1.0	85 ± 1.4	122 ± 2	310 ± 6	1930 ± 60	3710 ± 140	10,900 ± 700
Theoretical stiffness, k_{theory} (N/m)	80 ± 21	102 ± 27	137 ± 37	562 ± 151	3190 ± 850	3500 ± 940	10,600 ± 2800

Length measurements were made in an optical microscope with a resolution of 0.5 μm. The measurements were fit to Euler beam theory (Eq. 1) to quantify Young's modulus, which was subsequently used to back-solve for the theoretical stiffness of each cantilever. The best-fit to modulus was 120 ± 32 GPa; our uncertainty analysis showed that ~ 90% of this error is attributable to uncertainty in the thickness measurement (~ 5% due to uncertainty in length and ~ 5% due to uncertainty in the calibrated spring constant). This modulus error was subsequently propagated into the theoretical stiffness calculation

2.2 Quantifying Cantilever Flexural Stiffness: The Direct Calibration Method

We adapted the nano-force calibrator (NFC) methods described by Kim *et al*. as a direct and traceable means for calibrating flexural stiffness [31]. The custom system we constructed is functionally analogous to the NFC and is shown schematically in Fig. 2. Briefly, the calibration system used a high-resolution (± 6 nm) nanopositioning stage (Physik Instrumente Q-545) to actuate the cantilever and a high sensitivity (± 100 nN) analytical microbalance (Mettler Toledo XP105DR®) to quantify the force response to cantilever deformations. A digital optical microscope with a 5 MP CMOS image sensor (Dino-Lite Edge AM7915MZTL) was used to guide the approach to contact (Fig. 2c). To perform a flexural stiffness calibration measurement, the probe was loaded and unloaded against a silicon flat, which was glued to a platform and mated with the microbalance tray at three contact points; three load-unload curves were used for each measurement. Linear regression of force versus actuation depth was used to quantify the spring constant and its statistical uncertainty. Three independent repeat measurements were performed with one soft (Lever 1–78 N/m) and one stiff cantilever (Lever 7–10,900 N/m) to quantify repeatability error from user–system interaction. For repeat measurements, the holder was removed from the instrument and the chip was removed from the holder before each repeat.

Because these analytical microbalances are self-compensating and extremely stiff, Kim et al. neglected any compliance from their NFC calibration system [31]. However, compliance of even stiff systems can become significant for stiff cantilevers similar to those of interest here. To correct for system compliance, we first quantified system stiffness, k_{system}, by repeating the calibration measurement with a Si blank in place of the cantilever. Five repeat measurements with independent blanks on independent days revealed that $k_{\text{system}} = 10{,}600 \pm 600$ N/m. The corrected stiffness of each cantilever was determined using the expression: $k_{\text{cantilever}} = \left({k_{\text{total}}}^{-1} - {k_{\text{system}}}^{-1}\right)^{-1}$. The total combined uncertainty in the cantilever spring constant was then quantified according to the Law of Propagation of Uncertainty as outlined by the ISO Guide to Uncertainty in Measurement [32].

2.3 Experimental Validation of Direct Calibration

Four Bruker CLFC-NOBO chips, each comprising three reference cantilevers, were used to experimentally validate the direct calibration method. Each tip-less reference cantilever was pre-calibrated by the manufacturer using the thermal tune method [33, 34] and had a nominal (prescribed) spring constant of 10.4, 1.3 or 0.16 N/m; specific pre-calibrated values were reported for each reference cantilever but experimental uncertainties in those values were not provided. Each cantilever chip was loaded into the custom holder and calibrated independently using the direct calibration method. Each direct calibration constant was compared against the manufacturer reported value to test agreement with a widely used industry standard.

2.4 Experimental Application

To quantify how substantially increased cantilever stiffness affects real-world normal and friction force sensing, we tested the colloid-stiffened cantilevers with a commercial AFM (Bruker Dimension 3100). The AFM normal force calibration constant (force per volts) depends on the cantilever-specific flexural stiffness (force per displacement) and the cantilever deflection sensitivity constant (volts per displacement), which can vary with differences in chip and laser positioning; for this reason, calibrations and measurements were done without changing chip or laser position in between. Cantilever deflection sensitivity calibration involved the regression of a single force–displacement curve

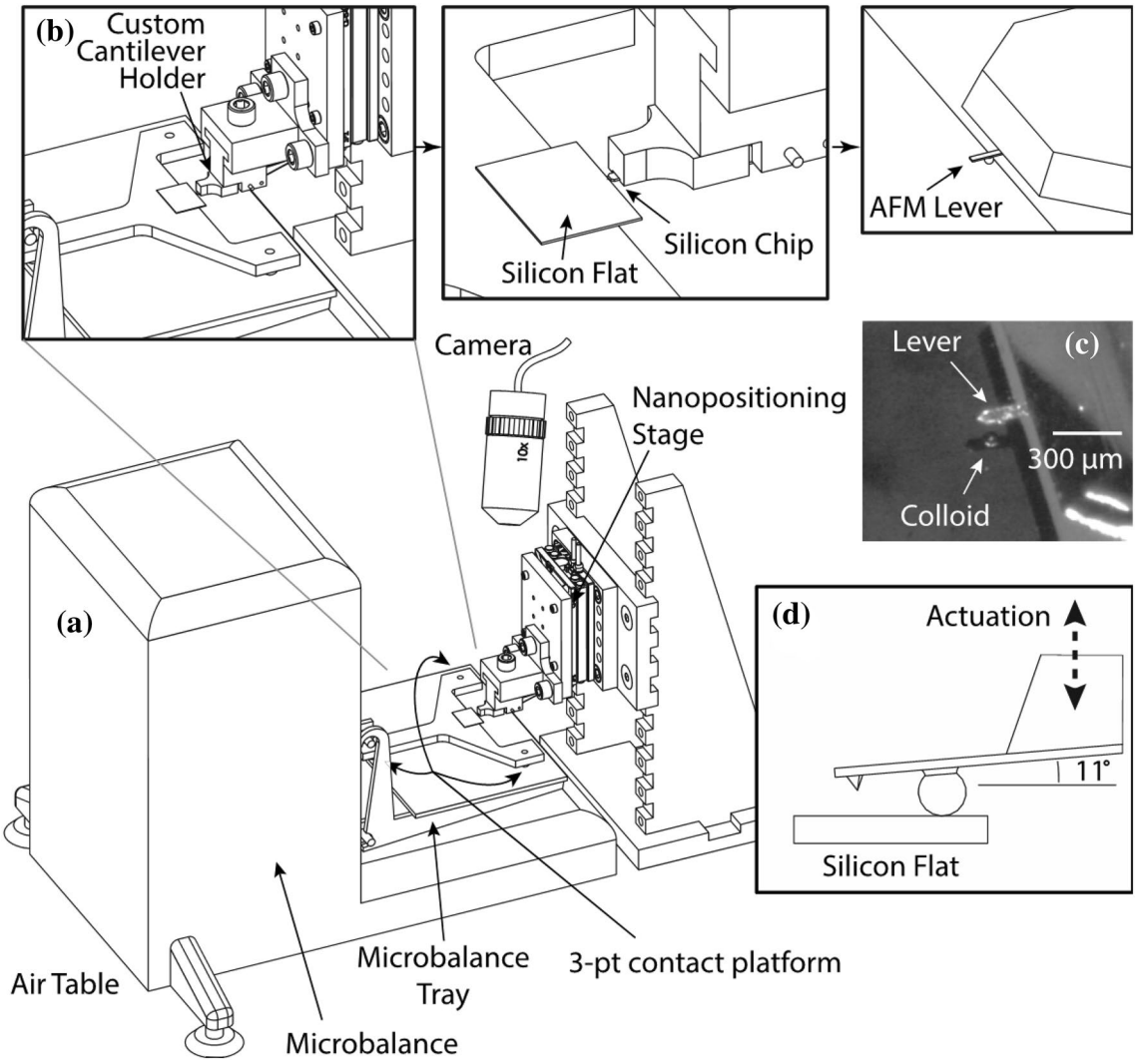

Fig. 2 **a** Schematic of the calibration setup; **b** close-up view of the contact between the AFM probe and the microbalance; **c** in situ view of the approach to contact; **d** Side-view of the silicon cantilever with a steel sphere mounted and loaded against the microbalance to obtain load–displacement relationships

of the test cantilever against a rigid Si substrate. The normal force calibration constant was determined as the product of the spring constant and the cantilever deflection sensitivity constant.

Application experiments were performed with one soft (Lever 3–122 N/m) and one stiff (Lever 7–10,900 N/m) cantilever. We tested our ability to detect low friction coefficients with colloid-stiffened cantilevers using single-crystal MoS_2, which, in the absence of gross wear, tends to produce low-friction coefficients on the order of 0.001–0.01 [35, 36] under varying experimental conditions. Friction loops (friction voltage versus position) were collected for varying set-point voltages from 0.5 to 8 V over a 5 µm by 5 µm scan window at 5 µm/s scan speed. The corresponding friction voltage and its uncertainty were determined by computing the mean and standard deviation of the half-width, respectively, over the middle 50% of the wear track; this 'reversal method' of friction analysis eliminates cross-talk effects (e.g., sensor misalignment, surface tilt, colloid offset) and artifacts from the reversal region (e.g., acceleration affects, static to kinetic transition, ringing, etc.) [37, 38]. We used the extended wedge method [36] immediately following testing to quantify lateral force calibration constants (per unit normal force calibration constant). Because the error sources in indirect model-based lateral force calibration approaches such as the extended wedge method are difficult to identify, we treat the resulting measurements as quantitative estimates.

3 Results

3.1 Validation of the Direct Calibration Method

Direct calibration curves for the three CLFC-NOBO reference cantilevers from a representative chip are shown in Fig. 3a. Measured flexural stiffness fits and the corresponding reported spring constants (red lines) are shown for reference. Mean values of flexural stiffness and uncertainty for all tested reference cantilevers (three cantilevers each on four chips) using direct calibration are shown in Fig. 3b, together with corresponding manufacturer-reported values of flexural stiffness. In general, the results demonstrate excellent quantitative agreement between the direct calibration method and the reported value. For the stiffest (11.3 N/m) and most compliant (0.19 N/m) cantilevers, differences between measured and reported values were less than 6% on average and can be attributed to the experimental uncertainty in the direct calibration measurement. Interestingly, we observed the worst agreement between measured and reported mean values (17% on average) for the intermediate beams (1.66 N/m). The differences, in this case, cannot reasonably be attributed to direct calibration uncertainty. There is circumstantial evidence that the differences are related to uncertainties in the reported values, which were not reported: (1) direct calibration constants were always closer to nominal constants than reported constants; (2) direct calibration constants exhibited less lever-to-lever variation than the reported constants; (3) the greatest disagreements between direct and reported constants were observed when reported constants also deviated most from nominal constants. Despite these small differences, the general quantitative agreement between methods provides a degree of independent validation for both.

3.2 Calibration of High-Force Cantilevers with Colloidal Probes

Direct calibration spring constants are shown for each mounted and unmounted cantilever in Fig. 4. The measured spring constants of unmodified cantilevers were between 30 and 50 N/m (40 N/m nominal). Mounting a colloid near the free end increased the spring constant by ~2x (cantilever 1), while mounting a colloid near the fixed end (cantilever 7) increased the spring constant by ~300×. Experimental uncertainty as a portion of each measurement increased with cantilever stiffness; calibration uncertainty was on the order of 1% the measured value for the softest beam and approached 10% the measured value for the stiffest beam (Table 1). The variabilities in repeat measurements were consistent with the corresponding experimental uncertainty. Overall, these results demonstrate that: (1) colloid placement provides a controllable means for increasing cantilever stiffness by several orders of magnitude; (2) direct calibration, which is traceable to force and displacement standards, is applicable to cantilevers between 0.1 and 10,000 N/m of flexural stiffness.

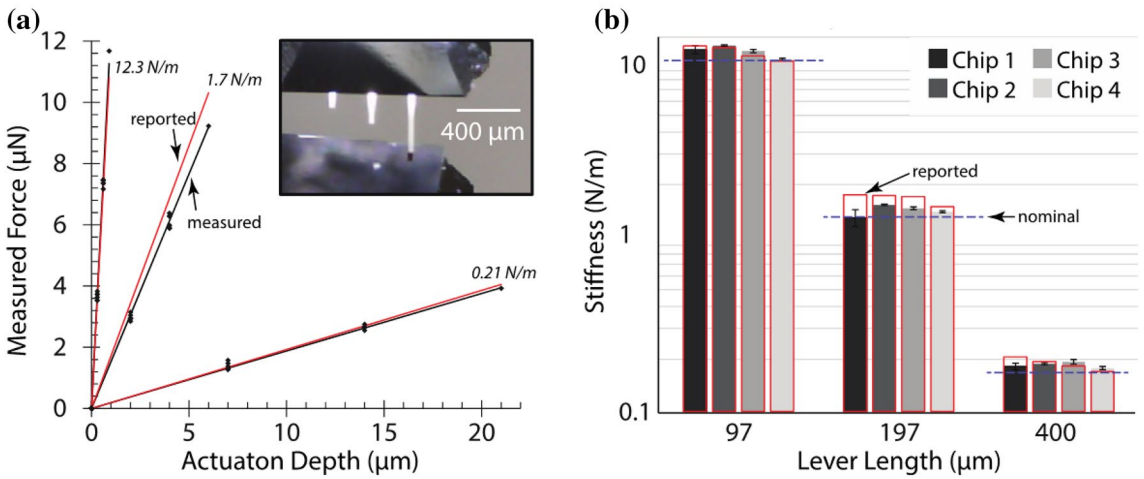

Fig. 3 **a** Stiffness curves for tip-less CLFC-NOBO reference cantilevers from a representative chip. Black dots represent measured data; black lines represent fits to measured data and are labeled by the corresponding slope; red lines represent the manufacturer-reported values from thermal-tuned calibration. Each curve represents the stiffness of a different cantilever on the same chip. The inset shows an in situ image of the long beam calibration measurement. **b** Results of direct calibration (shaded bars) with the long, medium, and short pre-calibrated cantilevers on each of four chips: nominal spring constants were 0.16, 1.3, and 10.4 N/m, respectively. Outlines (in red) represent the reporter value from pre-calibration and nominal values are denoted for each cantilever family by dashed lines. Error bars represent the uncertainties in direct calibration constants

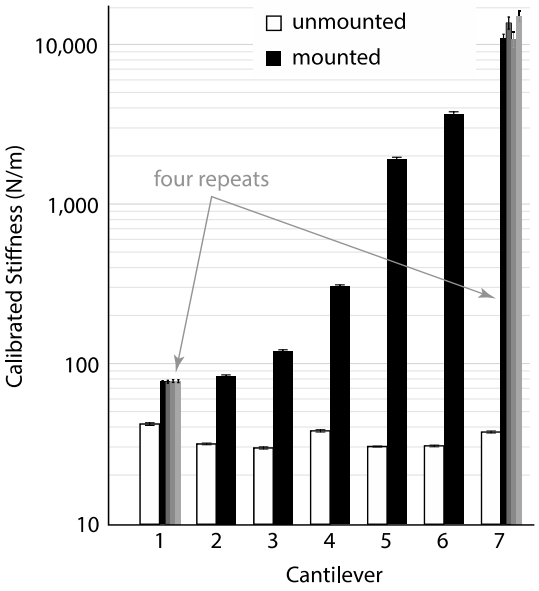

Fig. 4 Flexural stiffness from direct calibration for each of seven cantilevers before and after mounting the steel colloid. Error bars represent the statistical standard deviation in the slope of each independent calibration curve. Four independent repeat measurements were made for beams 1 and 7 to test for other error sources (e.g., lab temperature, chip placement in the holder, user repeatability, etc.). The consistency of the repeat results indicate that the experimental uncertainty is a reasonably comprehensive predictor of overall measurement error

Euler beam theory predicts that the stiffness is inversely proportional to the cube of the effective length per Eq. 1:

$$k_{\text{theory}} = \frac{3EI}{L^3} \tag{1}$$

The results in Fig. 5 agree well with the theory. Based on the measured variation in beam length, the expected variation in spring stiffness is $(107/21)^3 = 132\times$; the observed variation was $136\times$ (= 10,900/80 per Table 1). Plotting measured stiffness versus effective beam length gives a best fit with a power-law exponent of −3.03 and a coefficient of determination of 0.98 (Fig. 5a). Fitting the experimental measurements to beam theory yielded a Young's modulus of $E = 120 \pm 32$ GPa with $R^2 = 0.98$ (Fig. 5b); although the resulting modulus of E = 120 GPa is lower than the reported value of E = 169 GPa (for the <110> direction) [39], the difference is on the order of the fit uncertainty, ~90% of which is attributable to thickness uncertainty (0.5 µm). Thickness uncertainty also propagates unfavorably into flexural stiffness estimates (theoretical), which deviated from the measurements by ~50% on average. Although thickness uncertainty can be substantially reduced (e.g., with SEM measurements), other error sources are likely to emerge (e.g., stiffening and softening effects from the glue layer). Thus, we recommend quantifying beam stiffness with direct calibration when possible.

3.3 High-Force AFM

The cantilever deflection sensitivity calibration curves for a stiff and a soft cantilever are shown in Fig. 6a. Both cantilevers were subject to significant snap-in forces, pull-off forces, and hysteresis between loading and unloading. The PSD sensitivities (C_z), which were determined using the linear portion of the loading curves, were 25.2 ± 0.1 and

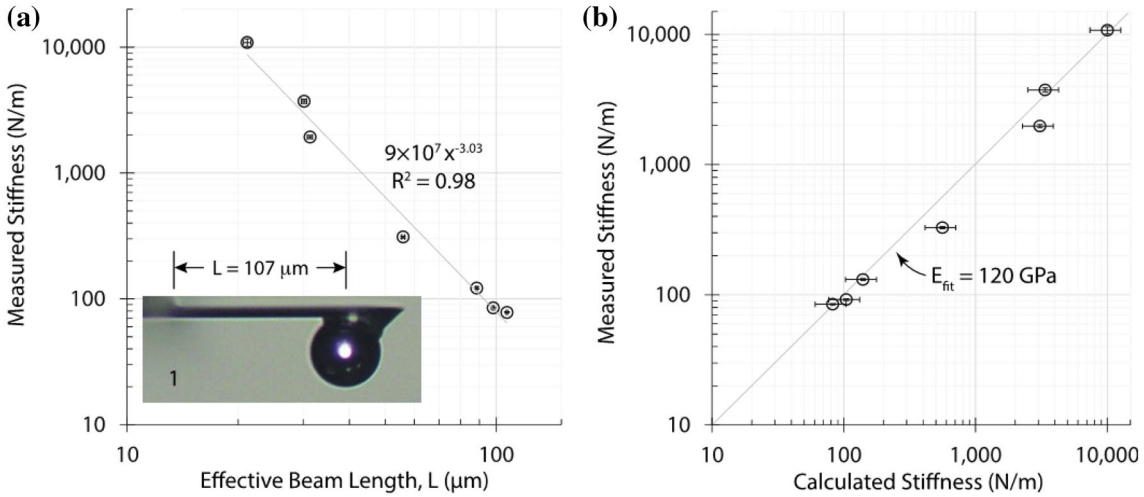

Fig. 5 **a** The measured stiffness for all eight beams plotted versus effective beam length, which is defined as the distance between the fixed end and the center of the colloid as illustrated with beam 1 in the inset. The results indicate strong agreement with the theoretical $k \sim length^{-3}$. **b** A comparison between measured stiffness using and stiffness calculated based on the dimensions obtained from side-view micrographs. The error bars in the measured stiffness represent the combined error in the regression and the error in the assembly's compliance while the error bars in the calculated stiffness reflect the propagation of errors from individual measurements into Eq. 1 (~90% from uncertainty in the thickness measurement)

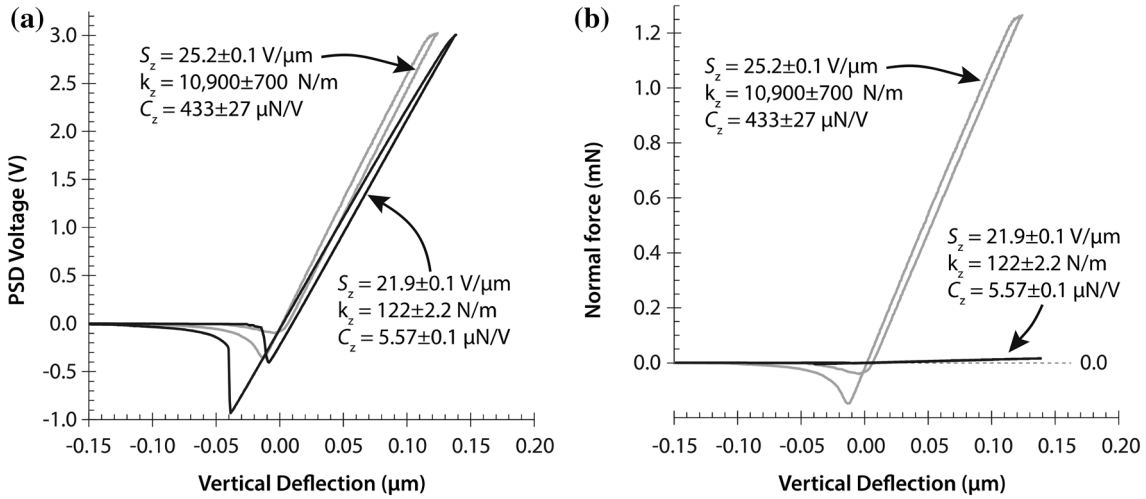

Fig. 6 **a** Indentation curves for cantilevers 1 and 7. The approach and retract curve show substantial snap-in and snap-out due to adhesive forces. The smooth sloped part of the loading curve was used to quantify the PSD sensitivity. **b** The same indentation curves but with PSD voltages converted into quantitative forces. We achieved forces well above our 1 mN target using setpoint voltages well-below the limit (3 of 20 V) of a commercial AFM

21.9 ± 0.1 V/µm for the stiff and soft cantilevers, respectively. The ~20% difference between these values is consistent with differences we have observed for repeat measurements of the same cantilever and indicates that spring constants can be modified radically without radically changing deflection sensitivity. For the stiffest cantilever, the resulting normal force calibration constant (ratio of stiffness and deflection sensitivity) of 433 µN/V reflects a possible measurement range of more than 8 mN (± 10V PSD range), which is well within the measurement range of existing microtribometers [40, 41]. For these calibration experiments, a set-point of only 3 V produced normal forces of 1.3 and 0.017 mN for stiff and soft beams, respectively (Fig. 6b). These results demonstrate that millinewton forces can be achieved in commercial AFM's using only existing materials and methods.

3.4 Lateral Force Sensitivity

Representative lateral voltage loops are shown for varying set-point voltages for a stiff cantilever (Lever 7) in Fig. 7a. Low friction between a steel colloid on single-crystal MoS_2 produced clean friction loops of statistically significant half-width at set-points down to 0.5 V. The tilt of the friction loop due to sample curvature increased with load, which suggests load-dependent deformation of the adhesive underlying the MoS_2 flake. We observed no evidence of load-induced curvature during follow-up testing against Si. It is also worth

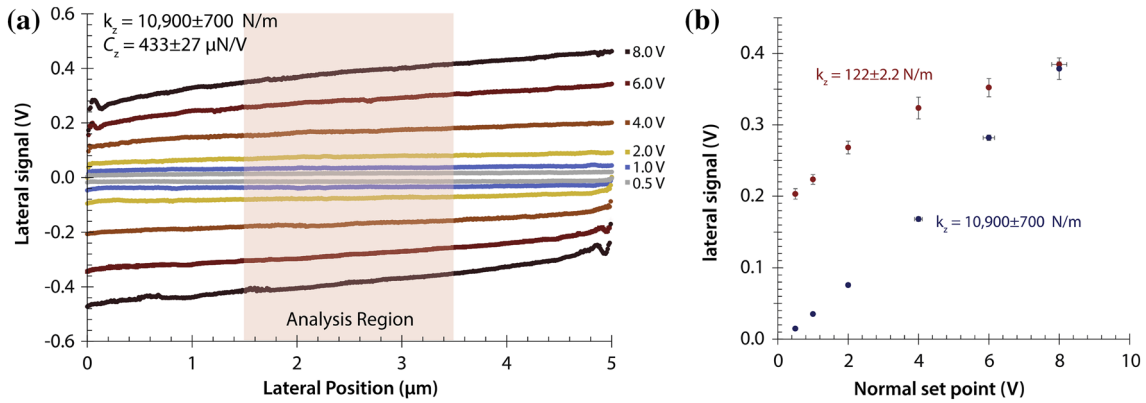

Fig. 7 **a** Friction versus position for set-point voltages from 0.5 to 8 V for a steel colloid against single-crystal MoS_2 using Lever 7, the stiffest cantilever in the study (k = 10,900 N/m). **b** Lateral signal (friction loop half-width) versus normal force set-point for a stiff (Lever 7, k = 10,900 N/m) and a soft (Lever 3, k = 122 N/m) cantilever. The application of friction to these beams produced similar voltage responses despite enormous differences in normal stiffness, torsional stiffness, and applied forces

noting that loops have been centered about zero for visual clarity; friction loop offsets arise in such measurements due to unavoidable misalignment between the sphere and the shear center of the cantilever in addition to other sources of cross-talk [36, 38].

The mean lateral signal, which is proportional to the friction force, is plotted versus normal set-point in Fig. 7b. Friction forces from nominally identical steel colloids sliding against the same MoS_2 sample at set-points between 0.5 and 8 V were well within the detectable range of the instrument for a stiff (Lever 7) and a soft (Lever 3) cantilever. Friction from the stiff cantilever was a linear function of load and passed approximately through the origin of the graph; both features are typical of macroscale contacts. Friction from the softer cantilever showed evidence of non-linearity and adhesive friction near zero load; these features are more typical of AFM-based friction measurements, especially when using colloidal spheres. These results suggest that the load regime has a significant effect on frictional behavior and demonstrate that beam-length modification can be used to study these effects in a controlled manner (e.g., same materials, geometries, speeds, etc.).

Calibrated friction forces are plotted versus normal force in Fig. 8 with linear fits for estimates of the corresponding friction coefficients. At low loads (~ 10 µN) and high loads (~ 1 mN), mean friction coefficients were ~ 0.009 and ~ 0.002, respectively, and consistent with previous measurements of single-crystal MoS_2 friction [35, 36]. Although both cantilevers produced comparable minimum friction forces, only the soft beam showed obvious evidence of adhesive friction approaching zero load (400 nN). In fact, the fit to friction results from the stiff cantilever gives a significant negative intercept (− 400 nN); it is worth noting that the pull-off force observed during PSD sensitivity calibration of this cantilever was ~ 100 µN. Together, the results are consistent with significant adhesive friction near zero load, decreasing friction coefficients with increasing load (sub-linear), and a transition toward linear behavior at the millinewton load regime. We are currently using these methods to better understand this transition behavior and how it depends on experimental variables such as load, probe radius, pressure, and cantilever stiffness.

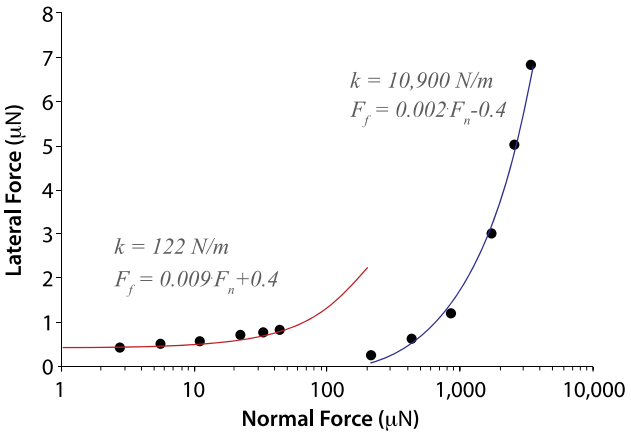

Fig. 8 Lateral force (per the extended wedge method) versus normal force for the stiffest ($k = 10{,}900$ N/m) and a soft ($k = 122$ N/m) cantilever in the study using two different steel colloid-attached probes and a MoS_2 sample. The relationship between friction force and normal force was obviously sub-linear at lower forces with the soft cantilever and closer to linear at higher forces with the stiff cantilever

4 Discussion

It can be argued that the most important grand challenge in tribology today is the gap in our understanding of macroscale friction phenomena and its underlying atomic-scale processes. Previous studies attempting to link macroscale and nanoscale friction results have done so by comparing them [24, 25, 27, 42, 43] rather than by joining them. To our knowledge, there have been no successful attempts to bridge this measurement gap directly within a single instrument or to match the experimental conditions between nanoscale and macroscale instruments (e.g., an AFM and a tribometer). This paper addresses existing experimental limitations by substantially increasing the accessible load range of commercial AFMs to the millinewton regime where it is possible for more traditional tribometers to operate [40, 44].

Mounting colloidal spheres near the fixed end of commercial cantilevers increased the effective spring constant by as much as 100×. Because these custom high-stiffness cantilevers are difficult to calibrate with confidence using more typical methods, we applied a direct method based on the nano-force calibrator (NFC) [31], which proved reproducible, flexible (from 0.1 and 10,000 N/m), and reliable (traceable to force and displacement standards). While direct calibration is best for quantitative studies, our results show that beam theory can be used to obtain reasonable estimates of cantilever stiffness, especially if dimensional uncertainties can be reduced to below 100 nm.

We demonstrate that the cantilevers fabricated for this study can be used to study friction of model systems such as single-crystal MoS_2 continuously and with significant overlap from 1 µN to 5 mN; such measurements will help elucidate how friction depends on both load and cantilever stiffness, the latter of which is likely both important and under-appreciated as an experimental variable [28]. Additionally, the load ranges of these AFM-based measurements overlap significantly with those available with more traditional tribometers, several of which have demonstrated the ability to resolve friction forces from comparably low friction material systems at normal forces well below 1 mN [40, 41]. Measurements from a tribometer are typically easier to

trace to calibration standards, serve as independent validation, and provide a direct path from mN forces to true macroscale tribological systems. We are now beginning to use the methods developed here in combination with a custom microtribometer (100 nN resolution) in an effort to bridge nanoscale and macroscale friction.

An unintended benefit of increased beam stiffness in the AFM is increased sensitivity to super-low friction coefficients. Friction forces for these low friction material systems can reach detection limits of multi-axial load cells whose orthogonal force sensitivities are comparable, which is often the case [45]. The transduction mechanisms of normal and friction forces in the AFM use different deformation modes, which effectively decouples orthogonal force sensitivities. Because torsional stiffness scales with length and normal stiffness with length cubed, sensitivity to low-friction coefficients increases with increased stiffness. The ratios between lateral and normal force calibration constants for soft (Lever 3) and stiff (Lever 7) cantilevers were $1.1/5.6 = 0.2$ and $9.3/433 = 0.02$, respectively, and effectively represent the ideal friction coefficient for each measurement system. It should be noted that the corresponding drawback is reduced range. Using a set-point of 8 V with the stiff Lever 7 would saturate the PSD at any friction coefficient greater than 0.025. Thus, larger friction coefficients will tend to limit the available load range when using this approach.

Finally, we would be remiss to neglect any comment on potential limitations from the AFM chip holder, the compliance of which reduces the normal force calibration constant by an unknowable amount without prior mechanical characterization. Separate stiffness measurements of our holder revealed no detectable indication of compliance ($k >> 30{,}000$ N/m) until forces exceeded the clip spring preload limit of ~ 10 mN where the spring constant fell to ~ 5000 N/m; it was a fortunate accident that our holder happened to be designed well for our target load range. While we assume that most AMF holders are of similar design and support comparable forces without significant confounding effects, we recommend characterizing the compliance profile of the AFM holder before attempting AFM measurements above 1 mN.

5 Conclusions

The data presented and analyzed here allow us to draw the following conclusions:

1) Colloid placement provides a controllable means for increasing the stiffness of commercial AFM cantilevers by more than two orders of magnitude.
2) Direct calibration, based on the nano-force calibrator (NFC) design described in a previous paper [31], is traceable to force and displacement standards, easily reproducible, and applicable to cantilevers between 0.1 and 10,000 N/m of flexural stiffness.
3) Mounting a colloid 21 μm from the fixed end of a 125-μm-long cantilever increased the stiffness by ~ 300×. In a Dimension 3100 AFM, the stiffened cantilever achieved normal forces of 3.4 mN while detecting friction forces from an ultra-low friction system (μ ~ 0.002). Stiffening the cantilever increased normal and lateral force calibration constants, while simultaneously improving sensitivity to ultra-low friction coefficients (i.e., as low as 0.001).

Acknowledgements N.T.G and D.L.B. acknowledge financial support from NSF Grant # CMMI-1434435. R.W.C. acknowledges support from NSF Grant # CMMI-1761874.

References

1. Tabor, D.: The area of contact between stationary and between moving surfaces. Doctoral Dissertation. University of Cambridge: (1939)
2. Sawyer, W.G., Argibay, N., Burris, D.L., Krick, B.A.: Mechanistic studies in friction and wear of bulk materials. Annu. Rev. Mater. Res. **44**, 395–427 (2014)
3. Bhushan, B.: Nanotribology and nanomechanics. Wear. **259**, 1507–1531 (2005)
4. Bhushan, B., Israelachvili, J.N., Landman, U.: Nanotribology: friction, wear and lubrication at the atomic scale. Nature. **374**, 607–616 (1995)
5. Carpick, R.W., Salmeron, M.: Scratching the surface: fundamental investigations of tribology with atomic force microscopy scratching the surface. Chem. Rev. **97**, 1163–1194 (1997)
6. Mate, C.M., McClelland, G.M., Erlandsson, R., Chiang, S.: Atomic-scale friction of a tungsten tip on a graphite surface. Phys. Rev. Lett. **59**, 1942–1945 (1987)
7. Tomlinson, G.A.: A molecular theory of friction. Lond. Edinb. Dublin Philos. Mag. J. Sci. 17, 147–56: (1929)
8. Prandtl, L.: Ein Gedankenmodell zur kinetischen Theorie der festen Körper. ZAMM J. Appl. Math. Mech. **8**, 85–106 (1928)
9. Bennewitz, R., Gnecco, E., Gyalog, T., Meyer, E.: Atomic friction studies on well-defined surfaces. Tribol. Lett. **10**, 51–56 (2001)
10. Bennewitz, R., Gyalog, T., Guggisberg, M., Bammerlin, M., Meyer, E., Güntherodt, H.J.: Atomic-scale stick-slip processes on Cu(111). Phys. Rev. B **60**, R11301–R11304 (1999)
11. Germann, G.J., Cohen, S.R., Neubauer, G., McClelland, G.M., Seki, H., Coulman, D.: Atomic scale friction of a diamond tip on diamond (100) and (111) surfaces. J. Appl. Phys. **73**, 163–167 (1993)
12. Dienwiebel, M., Verhoeven, G.S., Pradeep, N., Frenken, J.W.M., Heimberg, J.A., Zandbergen, H.W.: Superlubricity of graphite. Phys. Rev. Lett. **92**, 126101 (2004)
13. Park, J.Y., Ogletree, D.F., Salmeron, M., Jenks, C.J., Thiel, P.A., Brenner, J., Dubois, J.M.: Friction anisotropy: a unique and intrinsic property of decagonal quasicrystals. J. Mater. Res. **23**, 1488–1493 (2008)
14. Dienwiebel, M., Pradeep, N., Verhoeven, G.S., Zandbergen, H.W., Frenken, J.W.M.: Model experiments of superlubricity of graphite. Surf. Sci. **576**, 197–211 (2005)

15. Hirano, M., Shinjo, K., Kaneko, R., Murata, Y.: Observation of superlubricity by scanning tunneling microscopy. Phys. Rev. Lett. **78**, 1448–1451 (1997)
16. Brukman, M.J., Gao, G., Nemanich, R.J., Harrison, J.A.: Temperature dependence of single-asperity diamond-diamond friction elucidated using AFM and MD simulations. J. Phys. Chem. C **112**, 9358–9369 (2008)
17. He, M., Szuchmacher Blum, A., Overney, G., Overney, R.M.: Effect of interfacial liquid structuring on the coherence length in nanolubrication. Phys. Rev. Lett. **88**(15), 154302 (2002)
18. Schirmeisen, A., Jansen, L., Hölscher, H., Fuchs, H.: Temperature dependence of point contact friction on silicon. Appl. Phys. Lett. **88**(12), 123108 (2006)
19. Zhao, X., Hamilton, M., Sawyer, W.G., Perry, S.S.: Thermally activated friction. Tribol. Lett. **27**, 113–117 (2007)
20. Gnecco, E., Bennewitz, R., Gyalog, T., Loppacher, C., Bammerlin, M., Meyer, E., Güntherodt, H.J.: Velocity dependence of atomic friction. Phys. Rev. Lett. **84**, 1172–1175 (2000)
21. Baykara, M.Z., Vazirisereshk, M.R., Martini, A.: Emerging superlubricity: a review of the state of the art and perspectives on future research. Appl. Phys. Rev. **5**, 41102 (2018)
22. Sokoloff, J.B.: Theory of dynamical friction between idealized sliding surfaces. Surf. Sci. **144**, 267–272 (1984)
23. Gnecco, E., Bennewitz, R., Socoliuc, A., Meyer, E.: Friction and wear on the atomic scale. Wear. **254**, 859–862 (2003)
24. Yoon, E.S., Singh, R.A., Oh, H.J., Kong, H.: The effect of contact area on nano/micro-scale friction. Wear. **259**, 1424–1431 (2005)
25. Bhushan, B., Kulkarni, A.V.: Effect of normal load on microscale friction measurements. Thin Solid Films **278**, 49–56 (1996)
26. Nikhil, S.T.: Scale dependence of micro/ nano-friction and adhesion of mems/ nems materials, coatings and lubricants. Nanotechnology. **15**, 1561–1570 (2004)
27. Bhushan, B., Liu, H., Hsu, S.M.: Adhesion and friction studies of silicon and hydrophobic and low friction films and investigation of scale effects. J. Tribol. **126**, 583 (2004)
28. Liu, X.-Z., Ye, Z., Dong, Y., Egberts, P., Carpick, R.W., Martini, A.: Dynamics of atomic stick-slip friction examined with atomic force microscopy and atomistic simulations at overlapping speeds. Phys. Rev. Lett. **114**, 146102 (2015)
29. Khare, H.S., Lahouij, I., Jackson, A., Feng, G., Chen, Z., Cooper, G.D., Carpick, R.W.: Nanoscale generation of robust solid films from liquid-dispersed nanoparticles via in situ atomic force microscopy: growth kinetics and nanomechanical properties. ACS Appl. Mater. Interfaces. (2018)
30. Kappl, M., Butt, H.-J.: The colloidal probe technique and its application to adhesion force measurements. Part. Part. Syst. Charact. **19**, 129–143 (2002)
31. Kim, M.S., Cho, J.S. et al. Atomic force microscope cantilever calibration device for quantified force metrology at micro- or nano-scale regime: the nano force calibrator (NFC). Metrologia. **43**, 389 (2006)
32. Guide to the Expression of Uncertainty in Measurement, International Standards Organization (ISO). (1993)
33. Hutter, J.L., Bechhoefer, J.: Calibration of atomic-force microscope tips. Rev. Sci. Instrum. **64**, 1868–1873 (1993)
34. Butt, H.-J., Jaschke, M.: Calculation of thermal noise in atomic force microscopy. Nanotechnology. **6**, 1 (1995)
35. Zhao, X., Perry, S.S.: The role of water in modifying friction within MoS2 sliding interfaces. ACS Appl. Mater. Interfaces. **2**, 1444–1448 (2010)
36. Khare, H.S., Burris, D.L.: The extended wedge method: atomic force microscope friction calibration for improved tolerance to instrument misalignments, tip offset, and blunt probes. Rev. Sci. Instrum. **84**, 055108 (2013)
37. Burris, D.L., Sawyer, W.G.: Addressing practical challenges of low friction coefficient measurements. Tribol. Lett. **35**, 17–23 (2009)
38. Ogletree, D.F., Carpick, R.W., Salmeron, M.: Calibration of frictional forces in atomic force microscopy. Rev. Sci. Instrum. **67**, 3298 (1996)
39. Hopcroft, M.A., Nix, W.D., Kenny, T.W.: What is the young's modulus of silicon? J. Microelectromechanical Syst. **19**, 229–238 (2010)
40. Pitenis, A.A., Urueña, J.M., Hormel, T.T., Bhattacharjee, T., Niemi, S.R., Marshall, S.L., Hart, S.M., Schulze, K.D., Angelini, T.E., Sawyer, W.G.: Corneal cell friction: Survival, lubricity, tear films, and mucin production over extended duration in vitro studies. Biotribology. **11**, 77–83 (2017)
41. Marshall, S.L., Schulze, K.D., Hart, S.M., Urueña, J.M., McGhee, E.O., Bennett, A.I., Pitenis, A.A., O'Bryan, C.S., Angelini, T.E., Sawyer, W.G.: Spherically capped membrane probes for low contact pressure tribology. Biotribology. **11**, 69–72 (2017)
42. Bhushan, B., Nosonovsky, M.: Scale effects in friction using strain gradient plasticity and dislocation-assisted sliding (microslip). Acta Mater. **51**, 4331–4345 (2003)
43. Kanaga Karuppiah, K.S., Bruck, A.L., Sundararajan, S.: Evaluation of friction behavior and its contact-area dependence at the micro- and nano-scales. Tribol. Lett. **36**, 259 (2009)
44. Schulze, K.D., Bennett, A.I., Marshall, S., Rowe, K.G., Dunn, A.C.: Real area of contact in a soft transparent interface by particle exclusion microscopy. J. Tribol. **138**, 41404–41406 (2016)
45. Urueña, J.M., Pitenis, A.A., Nixon, R.M., Schulze, K.D., Angelini, T.E., Sawyer, G.W.: Mesh size control of polymer fluctuation lubrication in gemini hydrogels. Biotribology **1–2**, 24–29 (2015)